

SUPPORTING INFORMATION

High efficiency semitransparent perovskite solar cells containing 2D nanopore arrays prepared in a single step

Osama M. Alkhudhari^a, Amal Altujjar^a, Muhamad Z. Mokhtar^a, Ben F. Spencer^{a,b}, Qian Chen^a, Andrew G. Thomas^{a,b}, Nigel W. Hodson^c, Xuelian Wang^a, Patrick Hill^d, Janet Jacobs^e, Richard. J. Curry^e and Brian R. Saunders^{a,*}

a) Department of Materials, University of Manchester, MSS Tower, Manchester, M13 9PL, U.K.

b) Photon Science Institute and The Henry Royce Institute, University of Manchester, Manchester, M13 9PL, U.K.

c) BioAFM Facility, Faculty of Biology, Medicine and Health, Stopford Building, University of Manchester, Oxford Road, Manchester, M13 9PT, U.K.

d) School of Chemical Engineering and Analytical Science, University of Manchester, M13 9PL, U.K.

e) Photon Science Institute, Department of Electrical and Electronic Engineering, University of Manchester, Manchester, M13 9PL, U.K.

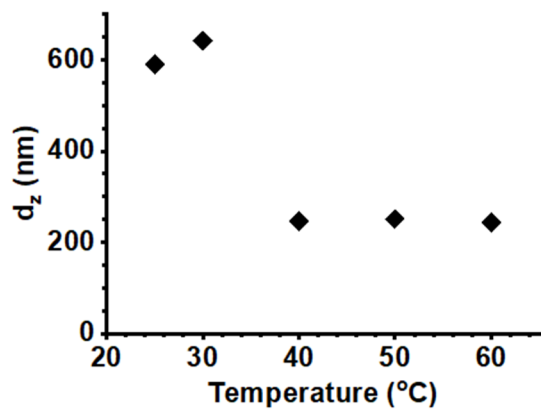


Figure S1. Temperature-dependent z -average diameter (d_z) of poly(*N*-isopropylacrylamide) microgels (PNP MG) in H_2O measured using dynamic light scattering (DLS).

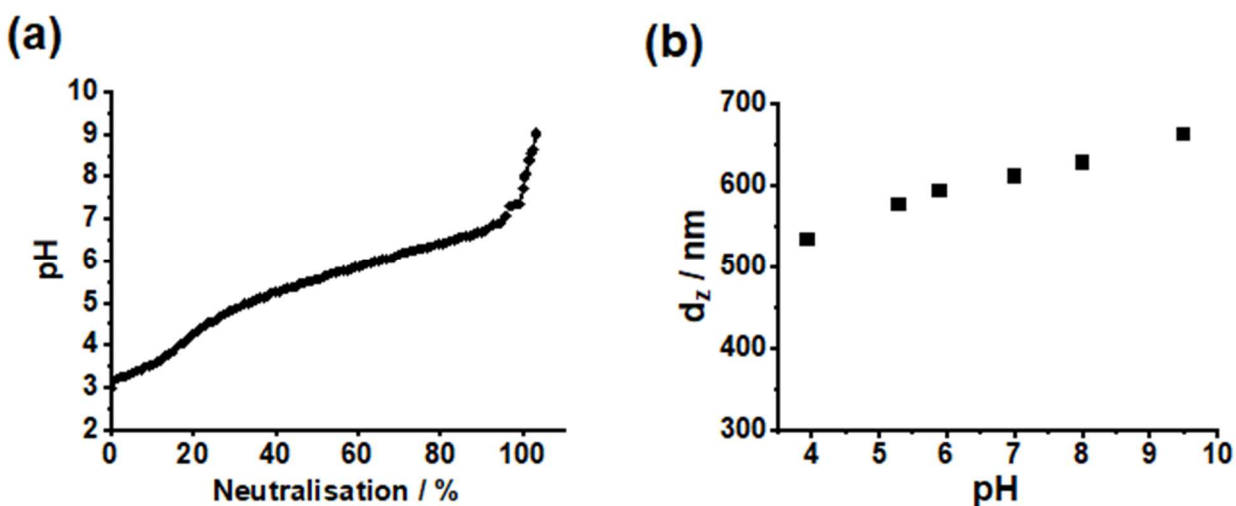


Figure S2. (a) Titration data for the PNP MG and (b) pH-dependent *z*-average diameter. The data were obtained at 25 °C. The effective pK_a is the pH corresponding to 50% neutralisation in (a).

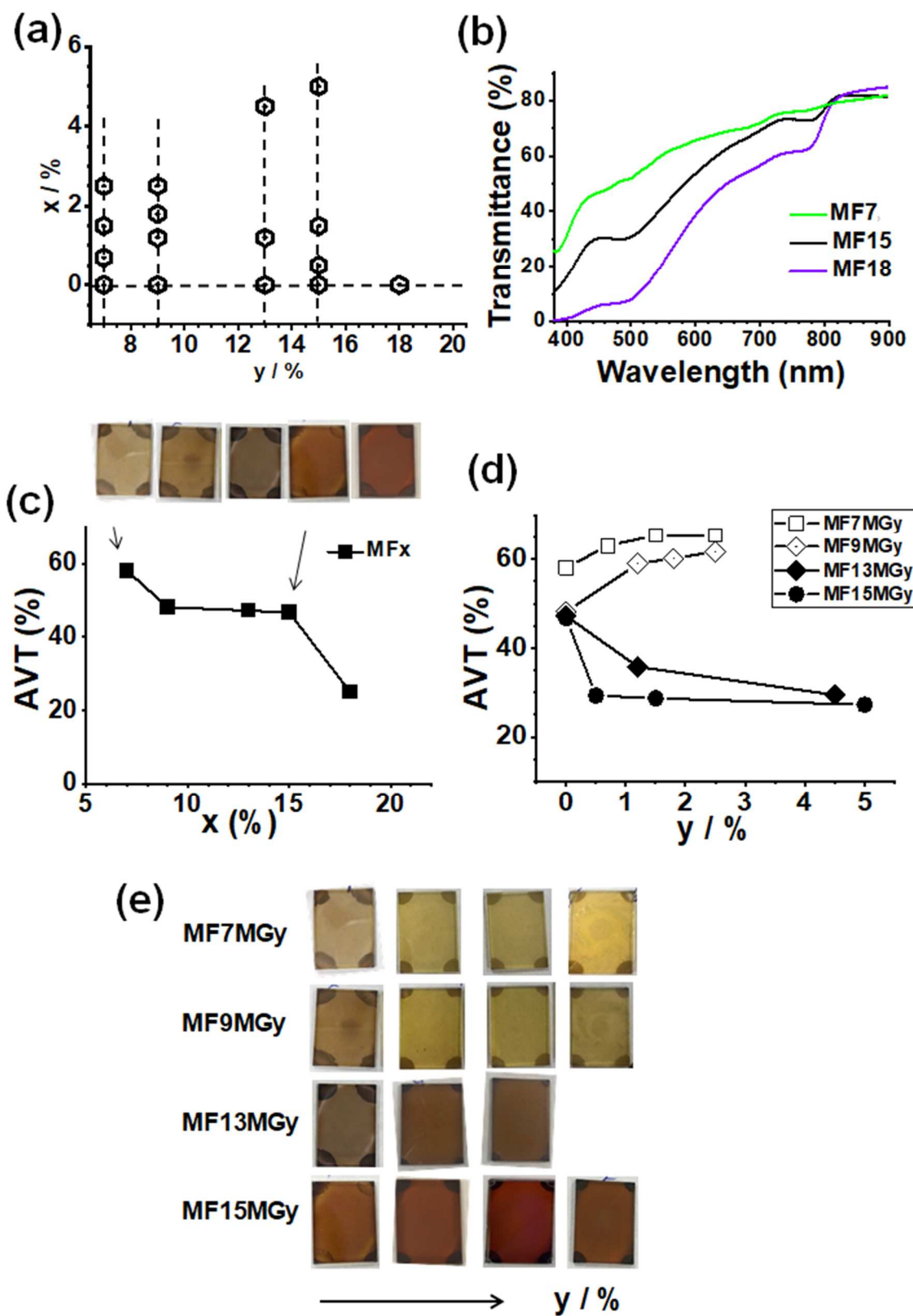


Figure S3. (a) MF x MGy film compositions used for AVT measurements. (b) Selected transmittance spectra for MF x films. (c) AVT values of the MF x films. Photographs of the films (20 mm x 15 mm) used are shown. (d) AVT values for the MF x MGy films plotted as a function of y . See Figure 8c for the spectra. (e) Photographs of the films used for (d).

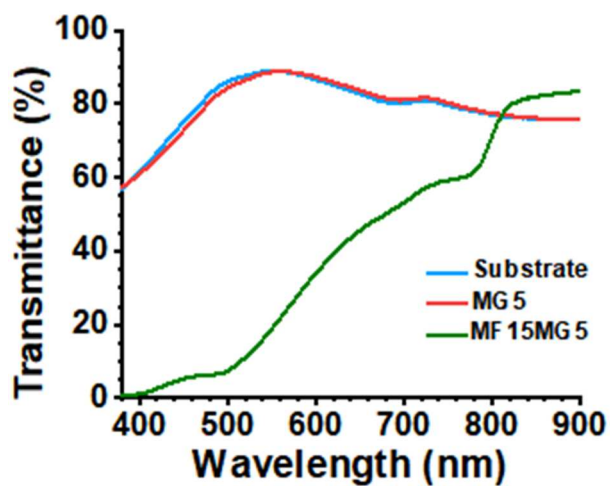


Figure S4. Transmittance spectra of MG5, MG15MG5 and the substrate (Glass/ITO/bl-TiO₂). There is no significant difference between the transmittance of the substrate with and without the MG5 film.

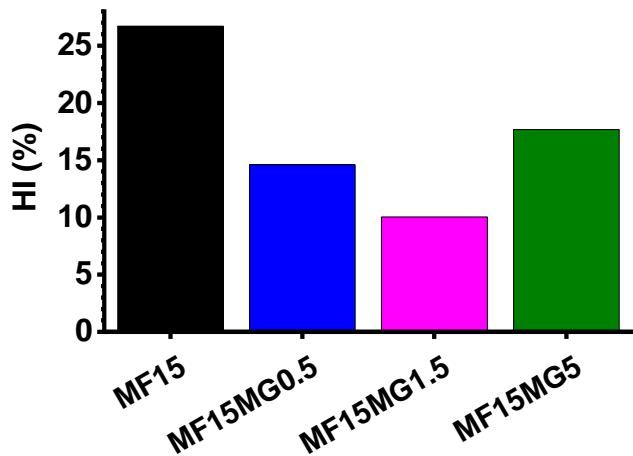


Figure S5. Hysteresis index (HI) values for the various devices. The latter values were calculated using: $HI = 100 \times [(PCE_{Rev} - PCE_{Fwd})/PCE_{Rev}]$.

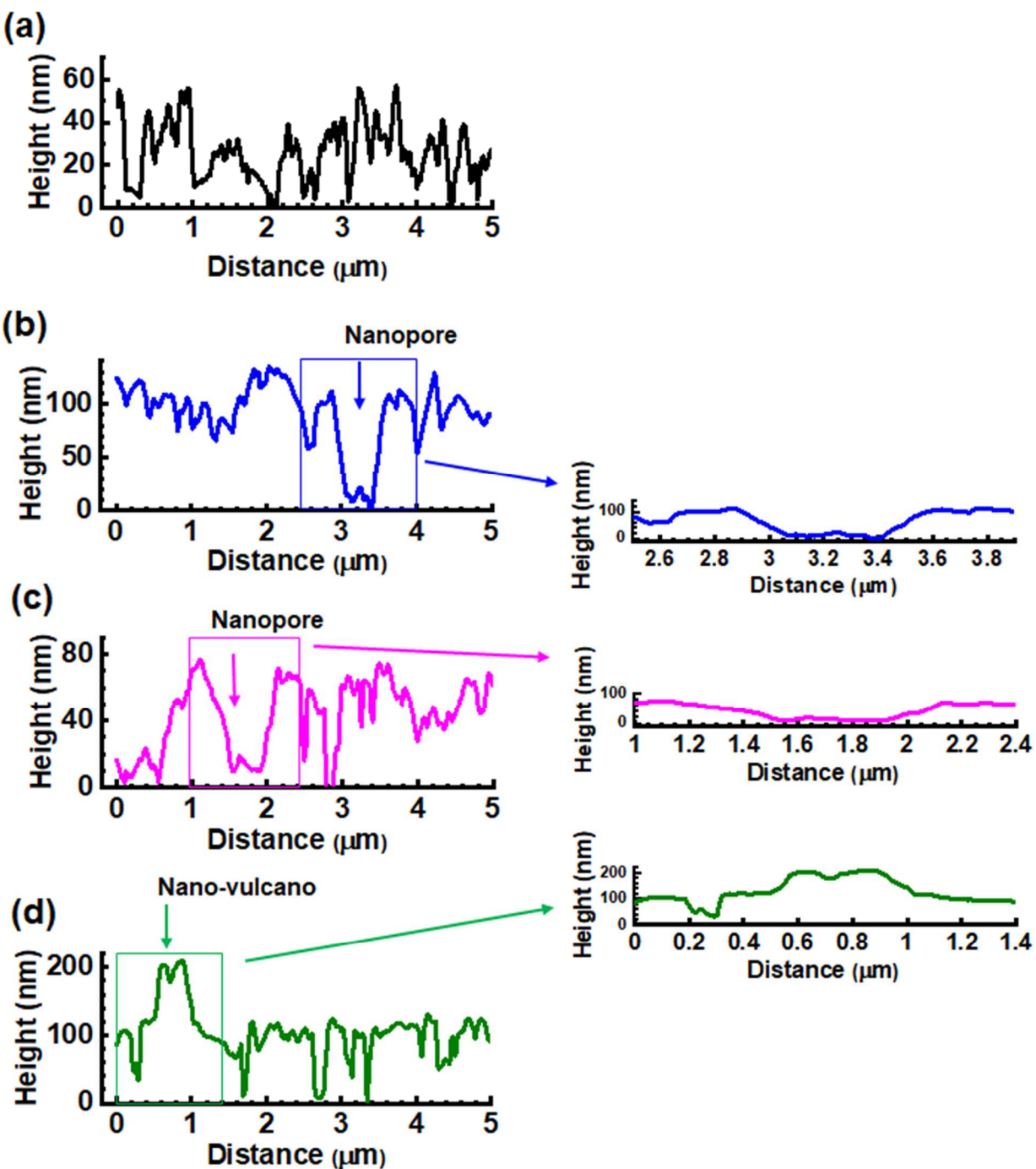


Figure S6. Line profiles for **(a)** MF15 **(b)** MF15MG0.5, **(c)** MF15MG1.5 and **(d)** MF15MG5.0.

Expanded views on the right-hand side show the highlighted features at a 1:1 scale.

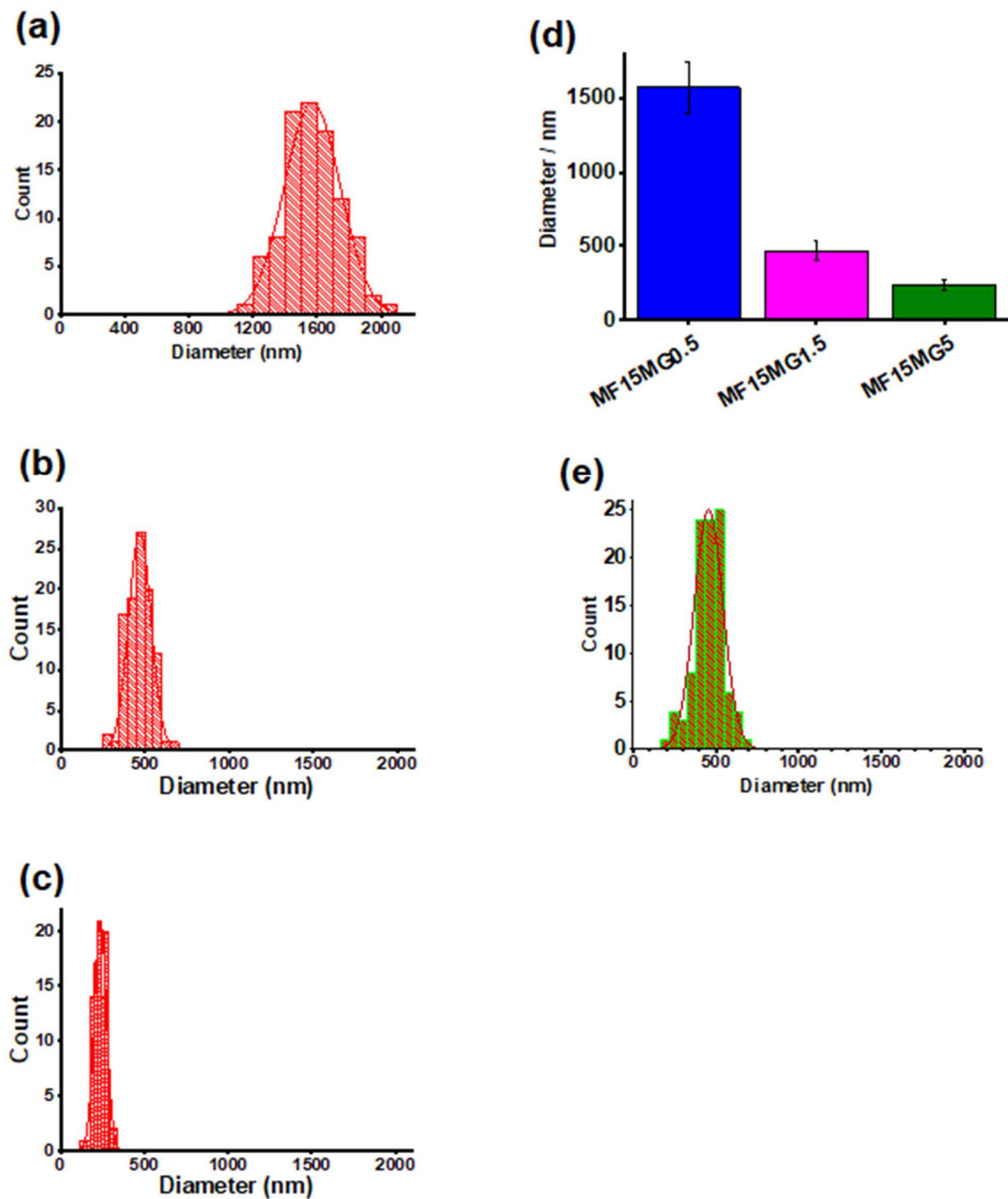


Figure S7. Nanopore diameter distribution measured for **(a)** MF15MG0.5, **(b)** MF15MG1.5 and **(c)** MF15MG5 from SEM. **(d)** Average nanopore diameters from (a) – (c). **(e)** Distribution of inner nanopore diameters for MF15MG0.5 measured from AFM. The average diameter is 456 ± 87 nm.

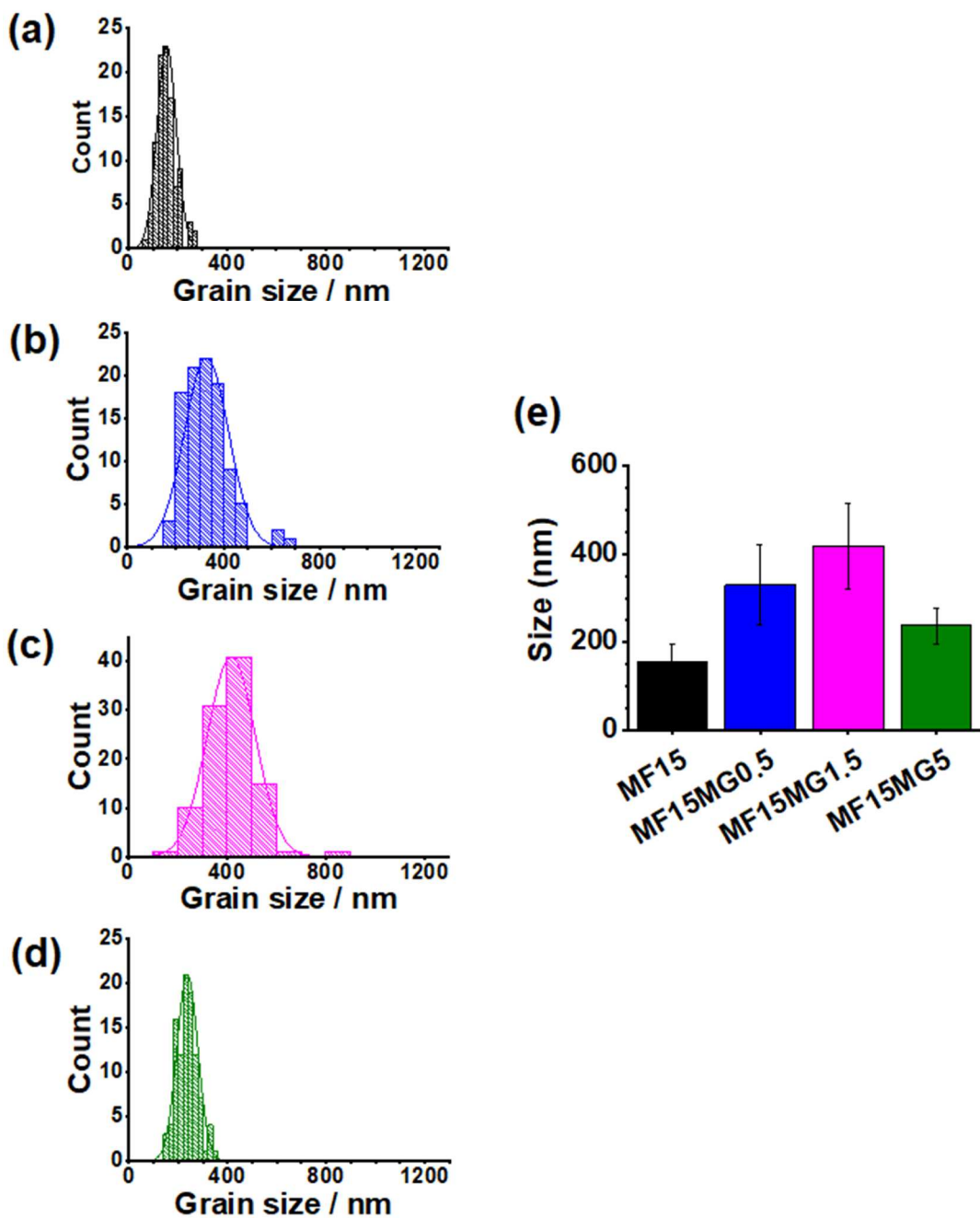


Figure S8. Grain size distributions ((a) – (d)) and average grain sizes (e) for the perovskite films.

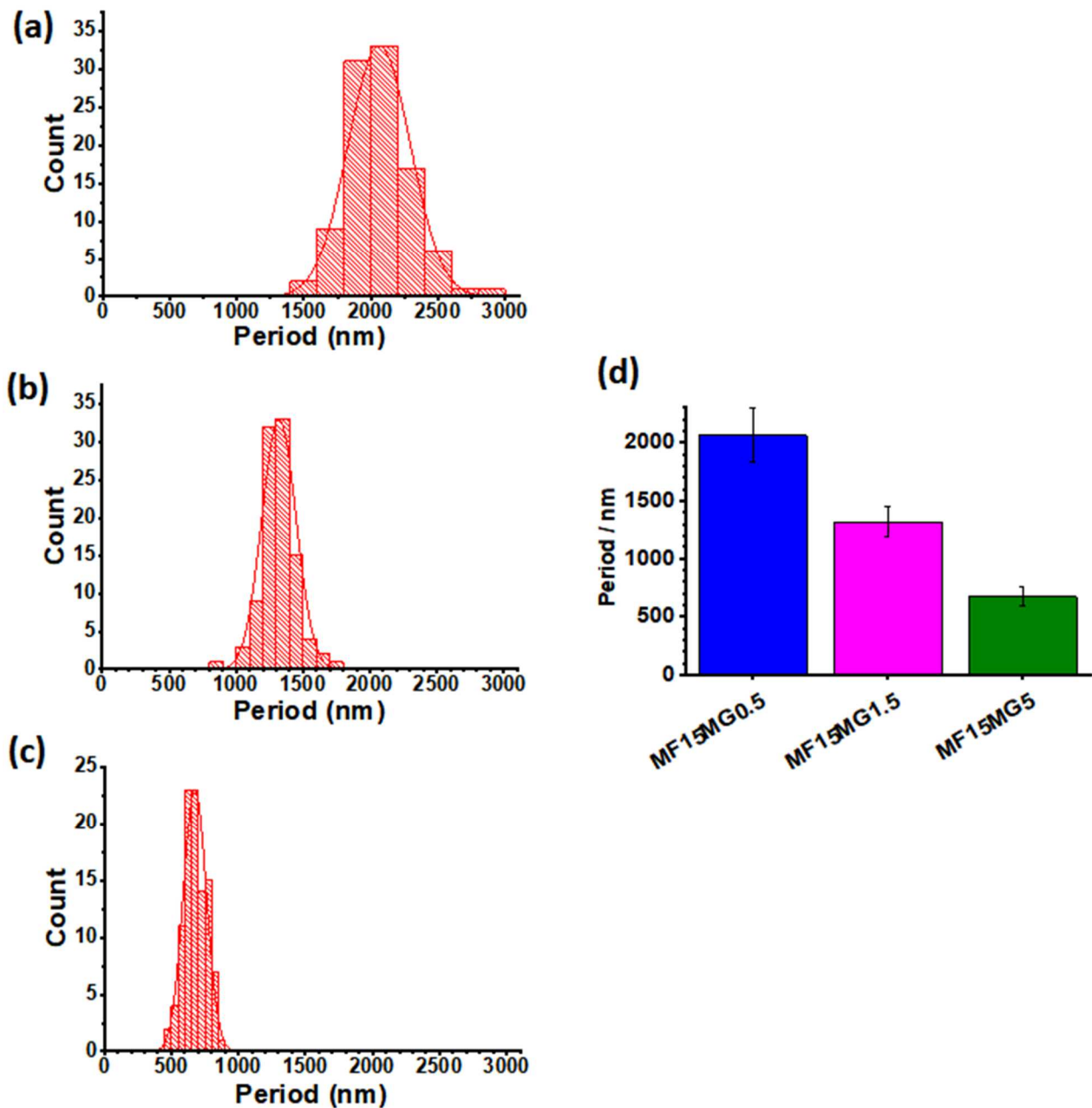


Figure S9. Center-to-center distance (period) distributions for the nanopores in **(a)** MF15MG0.5, **(b)** MF15MG1.5 and **(c)** MF15MG5 measured from SEM images. **(d)** Average period values from (a) to (c).

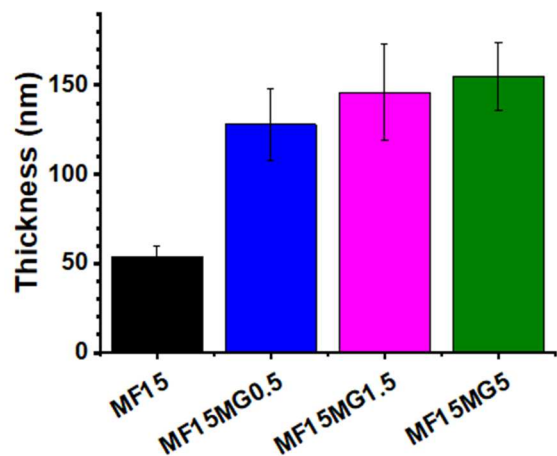


Figure S10. Thicknesses of the films studied determined from SEM cross-sections.

Discussion concerning the formation of 2D nanopore arrays in perovskite films

An interesting question concerns how the MGs can direct formation of the remarkably well-ordered 2D nanohole arrays evident from Figure 5. By extension of the current understanding of the mechanism for the deposition of non-close-packed hexagonal PNP NGs¹, the present MGs are likely initially adsorbed to the solvent-air interface at the beginning of spin-coating. They form hexagonally close-packed arrays with inter-MG spacing controlled by their initial (swollen) diameter as depicted in Figure S11. As the solvent evaporates the swollen MGs are deposited on the substrate and become immobilized. The MGs de-swell and flatten whilst preserving their original 2D array locations. Well-defined spaces form between the dried MGs due to MG de-swelling. As solvent further evaporates the perovskite crystals grow and the MGs flatten further. Crystal growth is restricted to the spaces between the deposited MGs and nanopores result. Hence, the hexagonal close-packing of MGs that existed at the solvent-air interfaces is transferred to hexagonal non-close-packing of 2D nanopores within the perovskite layer.

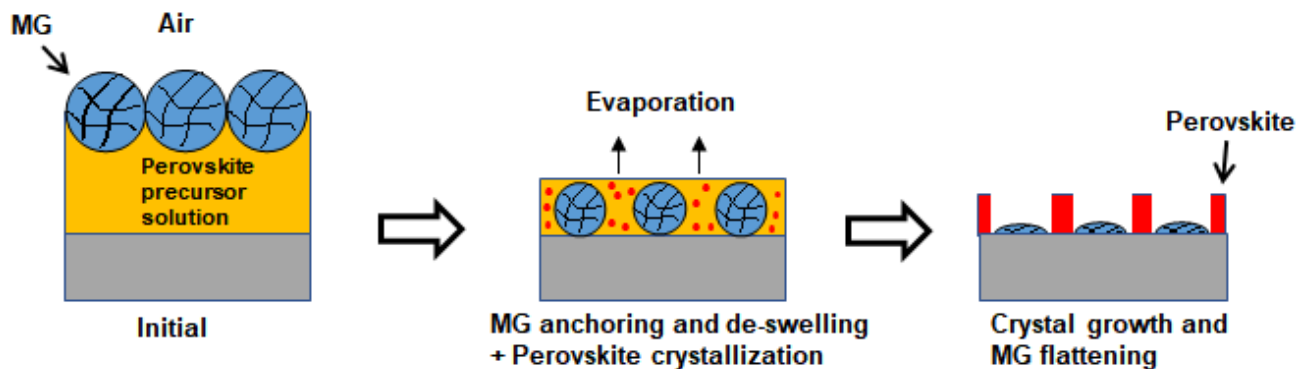


Figure S11. Depiction of proposed mechanism for formation of the perovskite films containing MG-templated nanopores.

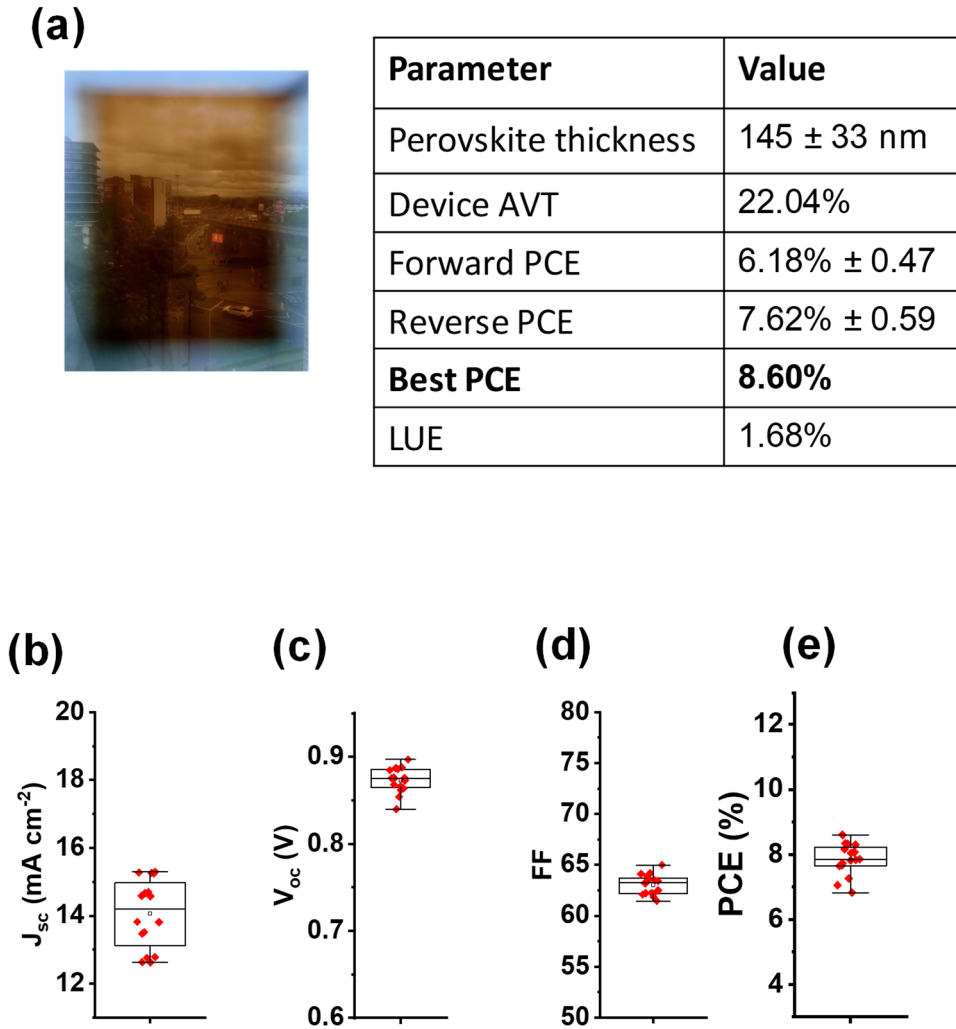


Figure S12. **(a)** Digital photograph of a MF18 STPSC and key parameters. The **(b)** short-circuit current density, **(c)** open circuit voltage, **(d)** fill factor and **(e)** power conversion efficiency data are shown for MF18 devices as box plots.

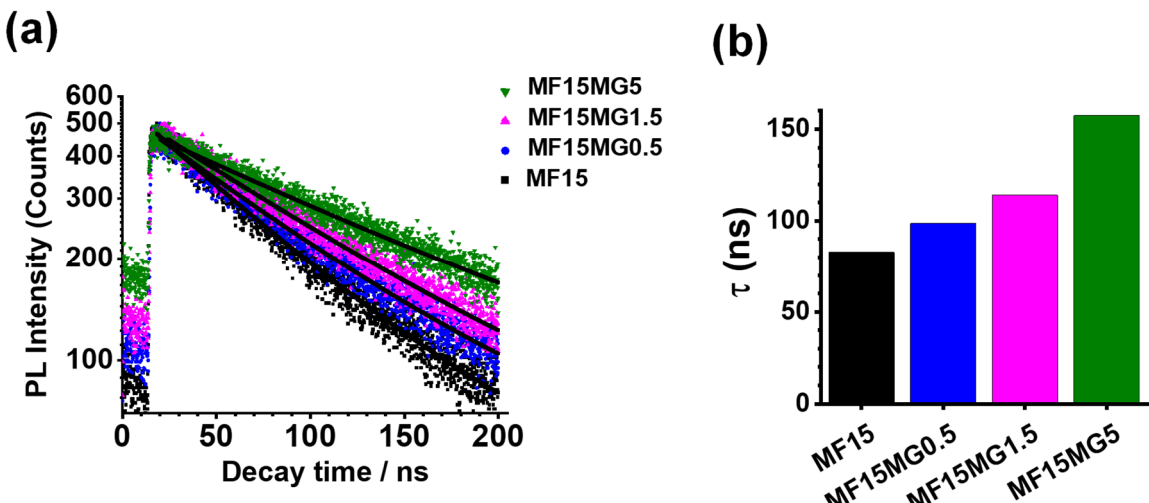


Figure S13. (a) Time-resolved PL profiles for the films and (b) decay time constants from the fits to the data shown in (a). The fits were obtained using $I_{PL} = A \exp(-t/\tau)$, where I_{PL} , A and τ are the PL intensity, pre-exponential factor and decay time constant, respectively. The A values for MF15, MF15MG0.5, MF15MG1.5 and MF15MG5 were 434, 412, 415 and 399 counts, respectively.

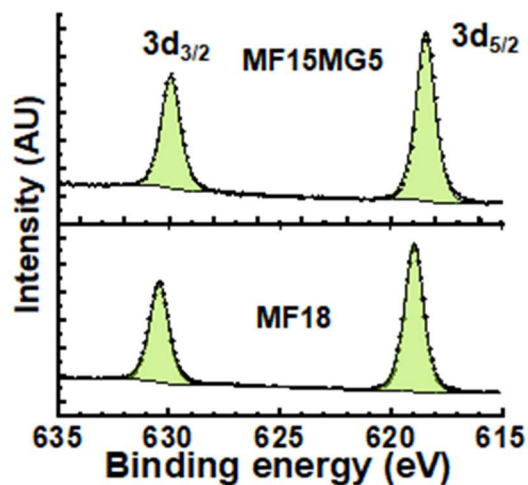


Figure S14. XPS 3d I core-level spectra for MF15MG5 and MF18.

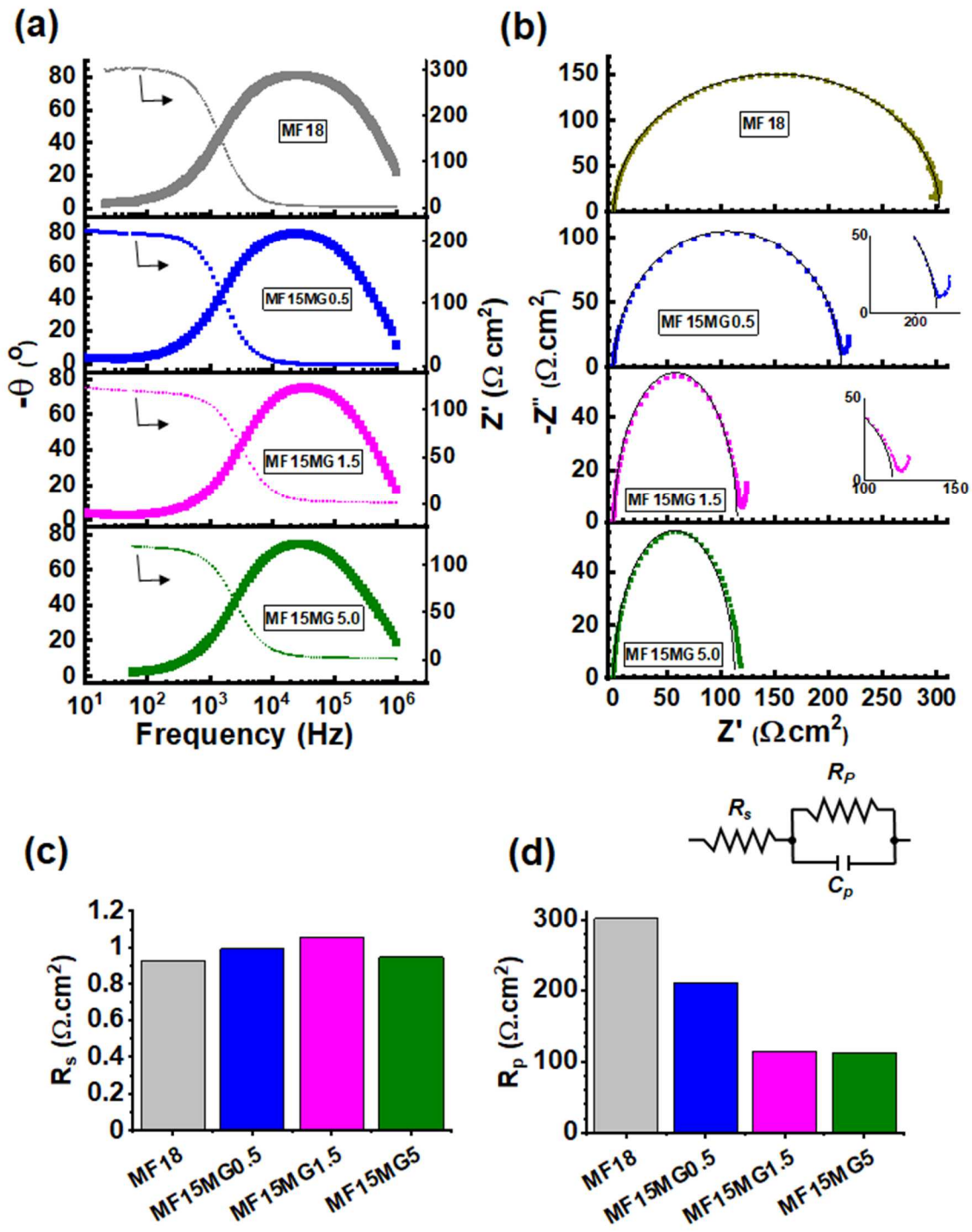


Figure S15. (a) Bode plots and (b) Nyquist plots for the devices. (c) and (d) show the series resistance (R_s) and parallel resistance (R_p) obtained by fitting the data using the circuit model shown in (d).

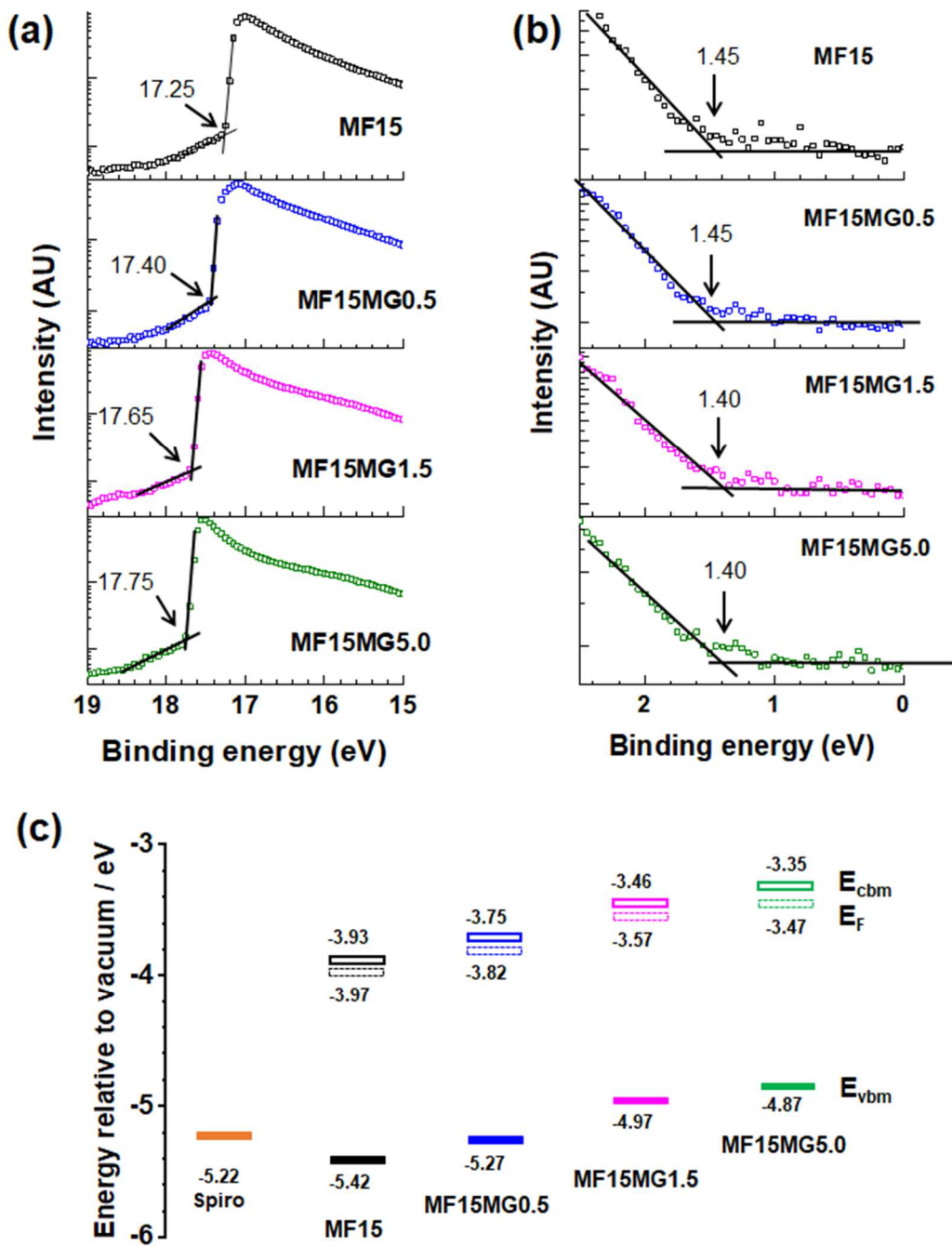


Figure S16. UPS spectra showing (a) the cut-off region and (b) the valence band edge region for the films. The work functions were obtained from the difference of $h\nu$ and the cut-off values in (a) and are equal in magnitude to the Fermi energy (E_F). The values for $E_{vbm} - E_F$ were obtained from (b) (v_{bm} is the valence band maximum). The conduction band minimum values (E_{cbm}) were obtained using the sum of E_{vbm} and E_g (from Fig. S17). (c) Band energy levels. The HOMO for Spiro is from Ref. 2.

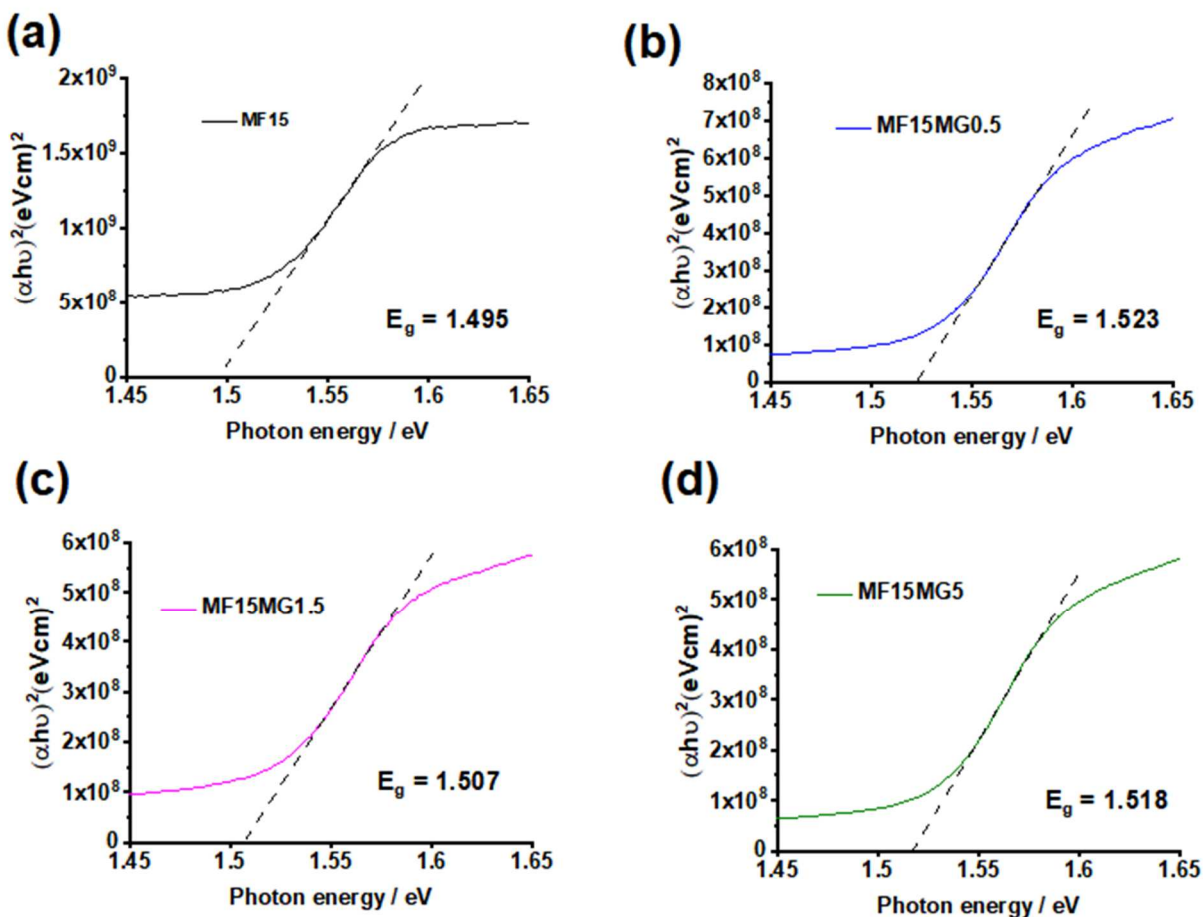


Figure S17. Tauc plots and optical band gap values for the studied films.

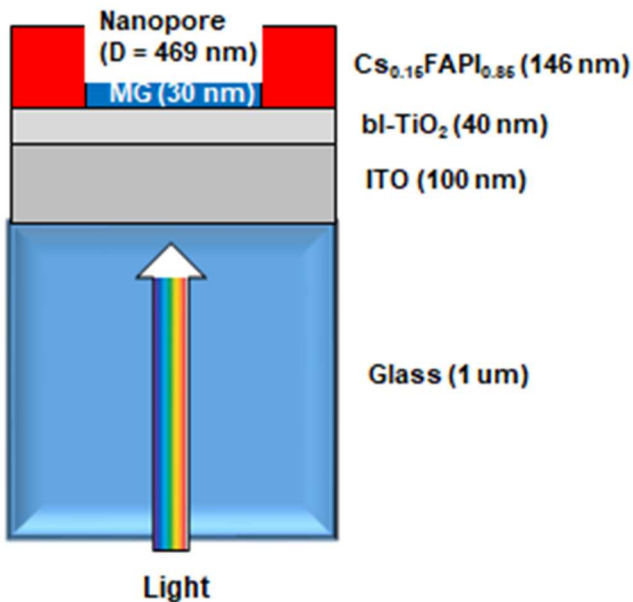


Figure S18. Depiction of the geometry used for the FDTD simulation of MF15MG1.5. The optical constants reported for Cs_{0.15}FAPbI_{0.85} were used for the simulation³. The nanopore diameter and layer thicknesses used are shown. See Table S4 for the other systems.

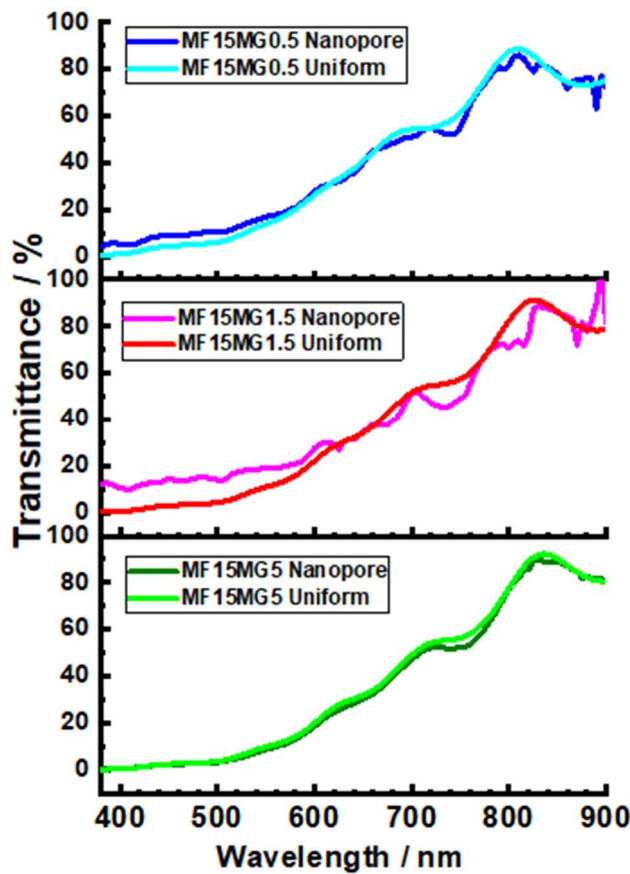


Figure S19. Simulated transmittance spectra for the MF15MGy films or MG-free uniform MF15 films with the same respective thickness.

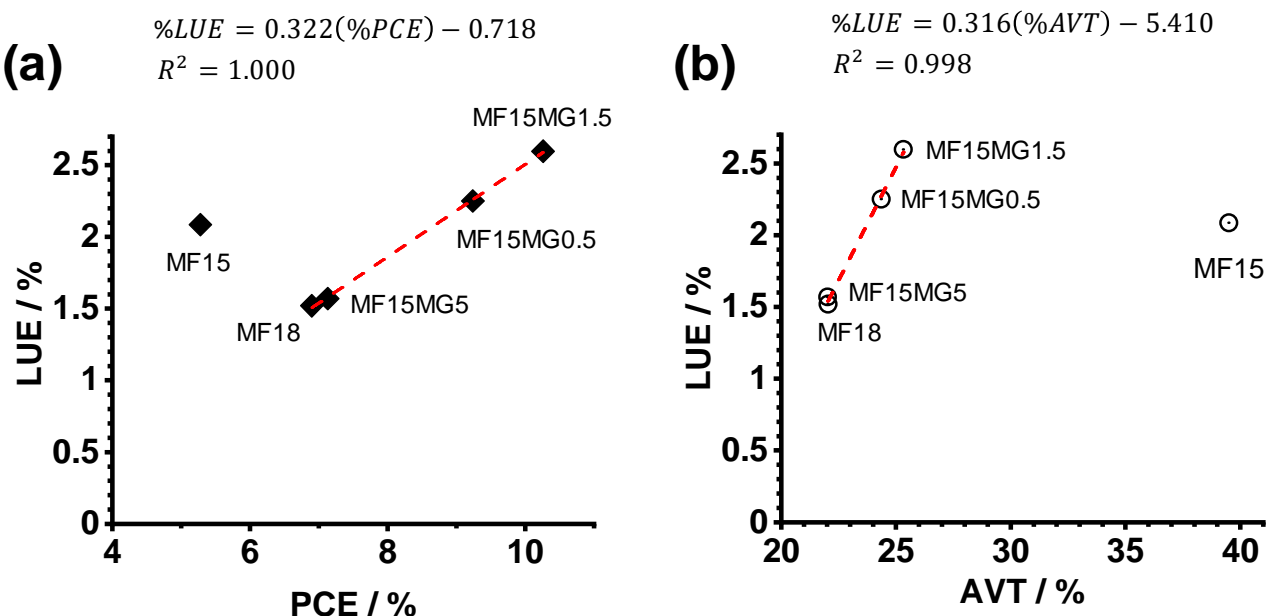


Figure S20. Variation of light utilization efficiency with (a) PCE and (b) AVT. The linear fits are applied to all the devices with the exception of MF15 (see text).

Table S1. Comparison of MG diameters measured under different conditions.

Solvent	d_z ^a /nm	PDI ^c
H ₂ O	590	0.003
DMF/DMSO	780	0.16

^a z-average diameter measured at 25 °C. ^c Polydispersity index.

Table S2. Photovoltaic parameters of the systems studied.

System	Scan direction	V _{oc} (Volts)	J _{sc} (mA.cm ⁻²)	FF (%)	PCE (%)
MF15	Forward	0.62 ± 0.009	14.22 ± 1.53	43.96 ± 0.81	3.87 ± 0.15
	Reverse	0.69 ± 0.009	14.17 ± 1.46	54.21 ± 0.65	5.28 ± 0.26
	Best	0.69	16.34	54.06	6.16
MF15MG0.5	Forward	0.83 ± 0.02	15.76 ± 0.32	59.61 ± 1.42	7.89 ± 0.39
	Reverse	0.89 ± 0.01	15.77 ± 0.30	65.71 ± 0.96	9.24 ± 0.34
	Best	0.90	16.07	66.43	9.68
MF15MG1.5	Forward	0.84 ± 0.03	17.23 ± 0.44	63.47 ± 2.83	9.23 ± 0.75
	Reverse	0.87 ± 0.02	17.13 ± 0.43	68.30 ± 4.27	10.26 ± 0.87
	Best	0.90	17.44	73.76	11.64
MF15MG5	Forward	0.75 ± 0.03	14.13 ± 0.67	55.06 ± 2.36	5.87 ± 0.43
	Reverse	0.82 ± 0.02	14.15 ± 0.67	61.13 ± 1.84	7.13 ± 0.42
	Best	0.83	14.94	62.88	7.82

Table S3. Summary of representative STPSCs.

Number in Fig. 3f	Top electrode	Device structure	PCE (%)	AVT (%)	Reference
R1	ITO	ITO/NiO _x /MAPbI ₃ //PCBM/AZO/ITO	12.52	11	4
R2	Cu	ITO/NiO _x /MAPbI ₃ /PCBM/PEIE/Cu	11.95	20	5
R3	IZTO	ITO/NiO _x /Cs _{0.175} FA _{0.75} MA _{0.075} Pb(I _{0.875} Br _{0.125}) ₃ /PMMA:PCBM/TS-IZTO	13.61	24.7	6
R4	BCP/Ag/MoO ₃	ITO/PEDOT:PSS/MAPbI ₃ /PCBM/AgNCs/BCP/Ag/MoO ₃	9.73	17.8	7
R5	AgNWs	ITO/PEDOT:PSS/MAPbI _{3-x} Cl _x /PCBM/ZnO/AgNWs	8.50	28.4	8
R6	AgNWs	ITO/PEDOT:PSS/MAPbI ₃ /PCBM/ALD ZnO/AgNWs/ALD Al ₂ O ₃ -coated PET	10.80	25.5	9
R7	Au	FTO/c-TiO ₂ /meso-TiO ₂ /Cs _{0.20} FA _{0.80} Pb(I _{0.6} Br _{0.4}) ₃ /Spiro/Au	10.03	28	10
R8	Ag	ITO/PEDOT:PSS/MAPbI ₃ /PCBM/C ₆₀ /AUH/Ag	9.40	29	11
R9	MoO ₃ /Au/MoO ₃	ITO/C ₆₀ /MAPbI _{3-x} Br _x /Spiro-OMeTAD/MoO ₃ / Au/MoO ₃	14.15	9	12
R10	MoO ₃ /Au/MoO ₃	FTO/SnO ₂ /C ₆₀ -SAM/Cs _{0.05} (MA _{0.15} FA _{0.85})Pb(I _{0.85} Br _{0.15}) ₃ /VNPB/MoO ₃ /Au/MoO ₃	16.10	10.1	13
R11	IZTO	ITO/NiO _x /MAPbI ₃ /PCBM/ZnO/IZTO	12.85	8.35	14
R12	Ag	FTO/c-TiO ₂ /PS-CM/SnO ₂ /MAPbI ₃ /Spiro-OMeTAD/Ag	10.30	38	15
R13	Au/LiF	ITO/PEDOT:PSS/polyTPD/MAPbI ₃ /PCBM/Au/LiF	6.4	29	16
R14	Au	FTO/c-TiO ₂ /meso-TiO ₂ +Al ₂ O ₃ NPs/MAPbI ₃ /Spiro-OMeTAD/Au	8	14.5	17
R15	Au	FTO/ c-TiO ₂ /FAPbI ₃ /SpiroOMeTAD/Au	6.4	33.6	18
R16	MoO ₃ /Au/MoO ₃	FTO/ c-TiO ₂ /MAPbI ₃ /Spiro-OMeTAD/MoO ₃ /Au /MoO ₃	13.6	7	19
R17	Ag	ITO/PEDOT:PSS/PVP/MAPbI _{3-x} Cl _x /CYTOP/PCBM/PEIE/Ag	5.36	34	20
R18	Ag/CsF	ITO/NiO _x /MAPbI ₃ /PCBM/Zr(acac) ₄ /Ag/CsF	11.74	23	21
R19	Au	FTO/c-TiO ₂ /AAO+ MAPbI _{3-x} Cl _x /Spiro-OMeTAD/Au	9.6	33.4	22
R20	Ag	ITO/PEDOT:PSS/MAPbI _{3-x} Cl _x /PCBM/D-ZnO/Ag	3.6	46	23
R21	Ag	FTO/c-TiO ₂ /MAPbI _{3-x} (SCN) _x /Spiro-OMeTAD/Ag	4.4	22.8	24
R22	Au	FTO/c-TiO ₂ /MAPbI ₃ •xCH ₃ NH ₂ /SWCNT/Ni Microgrid/PEDOT:PSS/Au	11.3	68	25

Table S4. Geometric parameters used for FDTD simulations of the MFxMGy films.

System	Thickness / nm	Nanopore diameter / nm	Period / nm	ϕ_{NPore}^a
MF15	54	-	-	-
MF15MG0.5	128	456 ^b	2060	0.04
MF15MG1.5	146	469	1320	0.11
MF15MG5	155	237	675	0.11

^a Fractional surface area occupied by the nanopores. ^b Average diameter from AFM data.

References

1. K. Horigome and D. Suzuki, *Langmuir*, 2012, **28**, 12962-12970.
2. N. J. Jeon, H. Na, E. H. Jung, T.-Y. Yang, Y. G. Lee, G. Kim, H.-W. Shin, S. Il Seok, J. Lee and J. Seo, *Nat. Energy*, 2018, **3**, 682-689.
3. P. F. Ndione, Z. Li and K. Zhu, *J. Mater. Chem. C*, 2016, **4**, 7775-7782.
4. M. B. Islam, M. Yanagida, Y. Shirai, Y. Nabetani and K. Miyano, *Sol. Energy Mater. Sol. Cells*, 2019, **195**, 323-329.
5. H.-J. Lee, S.-P. Cho, S.-i. Na and S.-S. Kim, *J. Alloys Compd.*, 2019, **797**, 65-73.
6. S.-H. Lim, H.-J. Seok, M.-J. Kwak, D.-H. Choi, S.-K. Kim, D.-H. Kim and H.-K. Kim, *Nano Energy*, 2021, **82**.
7. G. M. Kim and T. Tatsuma, *Sci. Rep.*, 2017, **7**, 10699.
8. F. Guo, H. Azimi, Y. Hou, T. Przybilla, M. Hu, C. Bronnbauer, S. Langner, E. Spiecker, K. Forberich and C. J. Brabec, *Nanoscale*, 2015, **7**, 1642-1649.
9. C.-Y. Chang, K.-T. Lee, W.-K. Huang, H.-Y. Siao and Y.-C. Chang, *Chem. Mater.*, 2015, **27**, 5122-5130.
10. M. Rai, S. Rahmany, S. S. Lim, S. Magdassi, L. H. Wong and L. Etgar, *J. Mater. Chem. A*, 2018, **6**, 23787-23796.
11. S. Bag and M. F. Durstock, *Nano Energy*, 2016, **30**, 542-548.
12. L. Yuan, Z. Wang, R. Duan, P. Huang, K. Zhang, Q. Chen, N. K. Allam, Y. Zhou, B. Song and Y. Li, *J. Mater. Chem. A*, 2018, **6**, 19696-19702.
13. J. C. Yu, J. Sun, N. Chandrasekaran, C. J. Dunn, A. S. R. Chesman and J. J. Jasieniak, *Nano Energy*, 2020, **71**.
14. Y.-J. Noh, J.-G. Kim, S.-S. Kim, H.-K. Kim and S.-I. Na, *J. Power Sources*, 2019, **437**.
15. L. Zhang, M. T. Hörantner, W. Zhang, Q. Yan and H. J. Snaith, *Sol. Energy Mater. Sol. Cells*, 2017, **160**, 193-202.
16. C. Roldán-Carmona, O. Malinkiewicz, R. Betancur, G. Longo, C. Momblona, F. Jaramillo,

- L. Camacho and H. J. Bolink, *Energy Environ. Sci.*, 2014, **7**, 2968-2973.
17. S. Rahmany, M. Layani, S. Magdassi and L. Etgar, *Sustainable Energy Fuels*, 2017, **1**, 2120-2127.
18. G. E. Eperon, D. Bryant, J. Troughton, S. D. Stranks, M. B. Johnston, T. Watson, D. A. Worsley and H. J. Snaith, *J Phys Chem Lett*, 2015, **6**, 129-138.
19. E. Della Gaspera, Y. Peng, Q. Hou, L. Spiccia, U. Bach, J. J. Jasieniak and Y.-B. Cheng, *Nano Energy*, 2015, **13**, 249-257.
20. Y. Guo, K. Shoyama, W. Sato and E. Nakamura, *Adv. Energy Mater.*, 2016, **6**.
21. Y.-W. Zhang, P.-P. Cheng, W.-Y. Tan and Y. Min, *Appl. Surf. Sci.*, 2021, **537**.
22. H.-C. Kwon, A. Kim, H. Lee, D. Lee, S. Jeong and J. Moon, *Adv. Energy Mater.*, 2016, **6**.
23. C. O. Ramírez Quiroz, I. Levchuk, C. Bronnbauer, M. Salvador, K. Forberich, T. Heumüller, Y. Hou, P. Schweizer, E. Spiecker and C. J. Brabec, *J. Mater. Chem. A*, 2015, **3**, 24071-24081.
24. S. Chen, B. Chen, X. Gao, B. Dong, H. Hu, K. Yan, W. Wen and D. Zou, *Sustainable Energy Fuels*, 2017, **1**, 1034-1040.
25. L. M. Wheeler, D. T. Moore, R. Ihly, N. J. Stanton, E. M. Miller, R. C. Tenent, J. L. Blackburn and N. R. Neale, *Nat Commun*, 2017, **8**, 1722.